NUMERICAL SIMULATIONS USING THE IMMERSED BOUNDARY TECHNIQUE

UGO PIOMELLI AND ELIAS BALARAS
Department of Mechanical Engineering
University of Maryland
College Park, MD 20742 - USA

Abstract. The immersed-boundary method can be used to simulate flows around complex geometries within a Cartesian grid. This method has been used quite extensively in low Reynolds-number flows, and is now being applied to turbulent flows more frequently. The technique will be discussed, and three applications of the method will be presented, with increasing complexity, to illustrate the potential and limitations of the method, and some of the directions for future work.

1. Introduction

The increase in computer speed achieved over the last few years has made computational fluid dynamics increasingly useful and widespread as a tool to analyze and design flow configuration. Complex geometries, however, present an obstacle even to present-day computers, since the use of body-fitted meshes (structured or unstructured) significantly increases the cost of a calculation in terms of both computational speed and memory requirements.

An alternative method that may be cost-efficient in many situations is the "immersed-boundary" method. This technique is based on the introduction of body forces distributed throughout the flow that mimic the effect that a solid body would have on the fluid. This approach allows the use of codes in Cartesian coordinates, which present significant advantages, in terms of speed, accuracy and flexibility, over codes that employ body fitted grids.

This idea has been widely used in hæmo-dynamics and bio-fluids engineering: two- and three-dimensional calculations of the flow in the heart

were reported by Peskin [13, 14] and McQueen and Peskin [8, 9]. In these calculations the motion of the boundary was determined by the fluid itself, so that the boundary had to be modeled as a set of elements linked by springs. In cases in which the boundary motion is known *a priori*, the problem can be significantly simplified.

Goldstein *et al.* [4] proposed a feedback forcing mechanism that forces the fluid velocity u_i to approach the velocity of the solid boundary, V_j, on the boundary itself. Consider the incompressible Navier-Stokes equations:

$$\frac{\partial u_j}{\partial x_j} = 0, \tag{1}$$

$$\frac{\partial u_i}{\partial t} + \frac{\partial}{\partial x_j}(u_j u_i) = -\frac{1}{\rho}\frac{\partial p}{\partial x_i} + \nu \nabla^2 u_i + f_i. \tag{2}$$

Goldstein *et al.* [4] assigned a force field

$$f_i(x_{s,i}, t) = \alpha_f \int_0^t \left[u_i(x_{s,i}, t) - V_i(x_{s,i}, t)\right] dt' + \beta_f \left[u_i(x_{s,i}, t) - V_i(x_{s,i}, t)\right], \tag{3}$$

where α_f and β_f are two negative constants, and $x_{s,i}$ are the coordinates of the solid surface. The net effect of this force is to tend to annihilate the velocity difference $u_i - V_i$. The flow, in fact, responds to the forcing as a damped oscillator (see [4] and [3] for an in-depth discussion of this issue); the frequency of the oscillator is $\propto |\alpha_f|^{1/2}$, whereas its damping coefficient is $\propto \beta_f / |\alpha|^{1/2}$. This implies that, in order to enforce the no-slip condition effectively, α_f and β_f must have large magnitudes (larger than the highest frequency in the flow), which may make the equations stiff.

Recently, Mohd-Yusof [11] proposed the "direct forcing method," which assigns a force field given by

$$f_i = \frac{\partial}{\partial x_j}(u_j u_i) + \frac{1}{\rho}\frac{\partial p}{\partial x_i} - \nu \nabla^2 u_i + \frac{V_i - u_i}{\Delta t}, \tag{4}$$

(where the dependence on $x_{s,i}$ and t has been omitted). This forcing imposes directly the desired velocity on the immersed boundary, and has the advantage (over the feedback forcing method) that it does not require significant reductions in the allowable time-step. It was extensively tested in a staggered finite-difference code by Fadlun *et al.* [3], who derived an interpolation scheme to be used when the boundary does not coincide with a grid line. Verzicco *et al.* [15] applied this method to the large-eddy simulation of high Reynolds number turbulent flows by calculating the flow inside an IC engine.

In the present paper additional applications of this method will be presented, and the potential and limitations of the technique, as well as issues

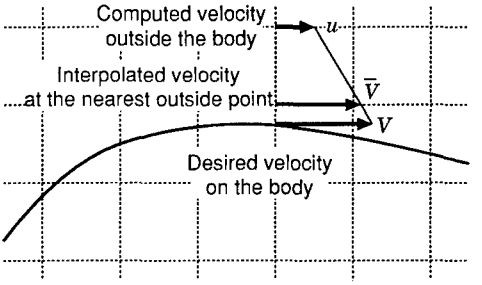

Figure 1. Interpolation method used to apply the forcing.

that require further study, will be discussed. After a brief review of the governing equations and of the numerical scheme used, three test cases will be shown: a low Reynolds-number flow over a cylinder in the presence of a moving surface (Wannier [16] flow), the flow over a circular cylinder at low Reynolds number, and the bypass transition on a flat plate caused by the interaction between the boundary layer and the wake of a circular cylinder.

2. Problem formulation

Governing the flow are the incompressible Navier-Stokes equations (1–2). The flow solver is a standard 2nd-order accurate method on a staggered mesh [1]. The fractional time-step method [2, 6] is used and a 2nd-order accurate Adams-Bashforth method is employed for the time advancement. A non-reflecting boundary condition [12] is used at the outflow, and periodic boundary conditions in the spanwise direction. The inflow and free-stream conditions depended on the case studied.

The direct forcing (4) was used. Since the immersed body does not follow a grid line the interpolation method proposed by Fadlun *et al.* [3] is used. The forcing is imposed not at the surface itself, but at the first point outside it (see Fig. 1) and the solid body velocity in (4) is replaced with the velocity $\overline{V_i}$ obtained by a linear interpolation between the computed fluid velocity outside the body, u_i, and the desired body velocity V_i. This method has several advantages: first, it has been shown to be fully second-order accurate in time [3]; therefore, it is consistent with the second-order differencing scheme used by the solver; secondly, since it assumes that the velocity profile is linear near the body, it implies homogeneous Neumann boundary conditions for the pressure (see the Appendix in [3] for a full discussion of this issue). This last feature is very important in the framework of fractional time-step methods, since it implies that the corrector step does not result in a modification of the body velocity imposed through the forcing in the Helmholtz step. On the other hand, the assumption that the velocity

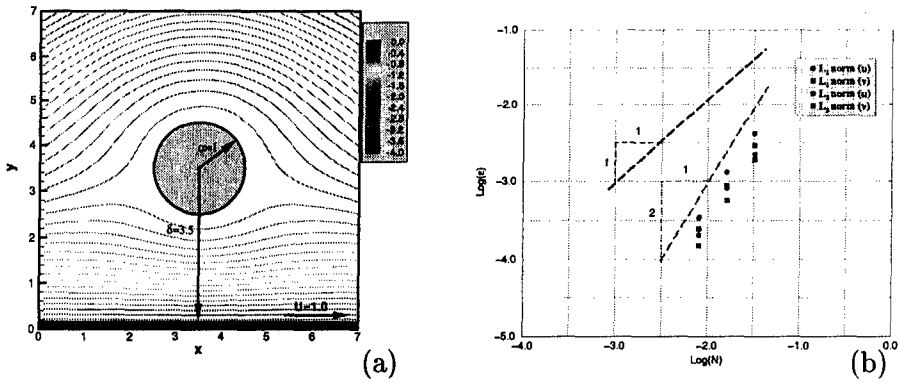

Figure 2. Wannier flow test case (Wannier 1950). (a) Computational domain and computed streamlines; (b) L_1 and L_2 norms of the error, ϵ, for u and v velocity components. N is the total number of grid points.

profile is linear over the first two layers of cells outside the immersed body requires the use of a very fine mesh in the vicinity of the body.

3. Results and discussion

3.1. WANNIER FLOW

A straightforward way to verify the accuracy of the proposed methodology is to compute a flow containing a curved immersed boundary for which an analytical solution exists. The case considered here is the Stokes flow around a cylinder in the vicinity of a moving wall (see Fig. 2). An analytical solution for this case was derived by Wannier [16]. The streamlines for this flow are shown in Fig. 2a. Three computations on gradually finer uniform grids (32×32, 64×64, and 128×128) were conducted. The L_1 and L_2 norms of the error (the difference between the computed and analytical solution) are shown in Fig. 2b as a function of the total number of points N. The error decreases with a -2 slope indicating that the proposed methodology is second order accurate.

3.2. FLOW OVER A CIRCULAR CYLINDER

The next test case examined is the flow over a circular cylinder at $Re_D = U_\infty D/\nu = 300$ (where D is the cylinder diameter and U_∞ the free-stream velocity). Two calculations will be compared: a 2D one that used 400×200 points in the $xz-$plane, and a 3D one, with the same mesh in the $xz-$plane, and 48 points in y. The computational domain was $60 \times 2\pi \times 30$, and the cylinder center was at $x_c = 10$, $z_c = 15$ (all lengths are made dimensionless by D, all velocities by U_∞). The grid was stretched both in the $x-$ and

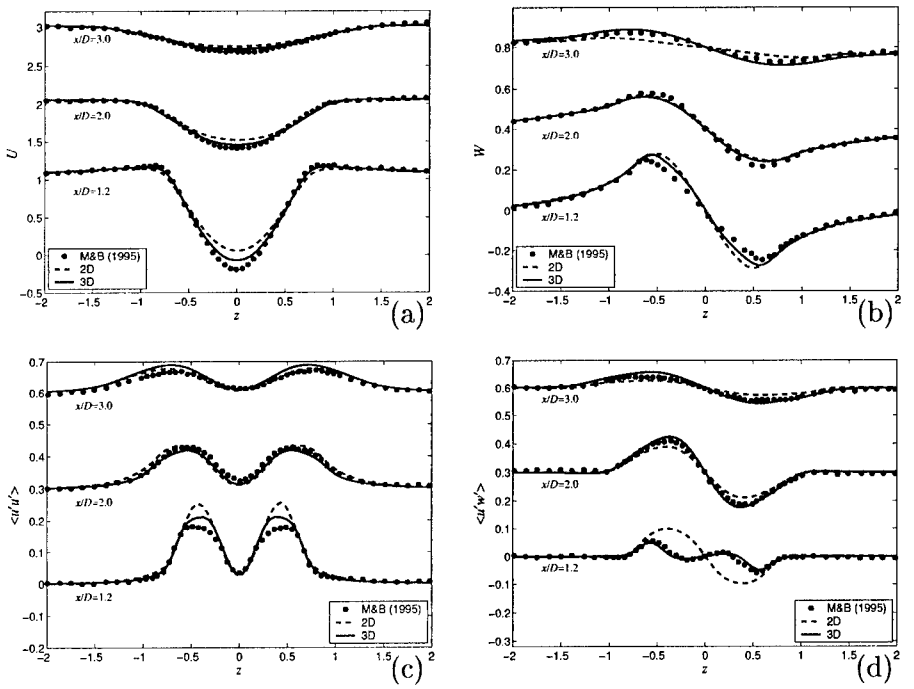

Figure 3. Flow over a circular cylinder, $Re_D = 300$. Velocity statistics. (a) U, (b) W, (c) $\langle u'u' \rangle$, (d) $\langle u'w' \rangle$. Reference data from Ref. [10].

$z-$directions; the last 1/6 of the domain (which required only 10 grid points in x) formed a sponge region, used to minimize the upstream propagation of disturbances due to the convective outflow conditions. A uniform velocity profile was imposed at the inlet, and slip-wall conditions were applied at $z = 0$ and $z = 30$.

The velocity statistics are shown in Fig. 3. Here and in the following the angle brackets denote averaging in time and in the spanwise direction. The 3D calculation is in very good agreement with the reference data by Mittal and Balachandar [10]. At this Reynolds number, three-dimensionality is observed in the wake, which is evidenced in the visualization in Fig. 4, which shows iso-surfaces of the second invariant of the velocity-gradient tensor,

$$Q = -\frac{1}{2}\frac{\partial u_i}{\partial x_j}\frac{\partial u_j}{\partial x_i} = -\frac{1}{2}\left(S_{ij}S_{ij} - \Omega_{ij}\Omega_{ij}\right), \tag{5}$$

(where $\overline{\Omega}_{ij}$ is the anti-symmetric part of the velocity gradient tensor). The condition $Q > 0$ identifies effectively the regions of coherent vorticity [5].

Figure 4 shows the formation of an instability on the initially 2D rollers, and the presence of quasi-streamwise rib vortices joining the rollers. The

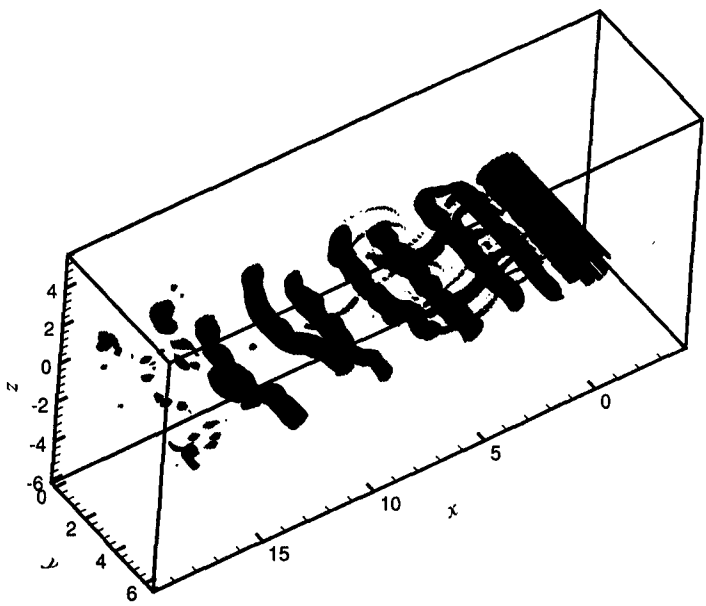

Figure 4. Flow over a circular cylinder, $Re_D = 300$. Isosurfaces of $Q = 0.6$.

magnitude of the spanwise Reynolds stresses $\langle v'v' \rangle$. in this calculation, however, remained significantly smaller than the other two normal components, which allowed the 2D calculation to give reasonable results.

The effects of the grid resolution near the obstacle are shown in Fig. 5. The cell Reynolds number is defined as

$$Re_c = \frac{(\Delta x^2 + \Delta z^2)\,(u^2 + w^2)}{\nu}, \tag{6}$$

where u and w are the instantaneous velocities, and Δx and Δz the grid spacings. If the mesh is insufficiently fine ($Re_c > 30$), some oscillations can be observed that initiate along lines at $\pm 45^o$ on the cylinder (they are especially visible in the w contours, Fig. 5b). Refining the grid, thus reducing Re_c reduces the size of this oscillation (Figs. 7a and b). Two-dimensional interpolation schemes that use both the points indicated by the diamonds and those indicated by squares in Fig. 6 to determine $\overline{V}_i$ have also been found (Verzicco, private communication, 2001) to reduce the amplitude of these oscillations.

3.3. WAKE/BOUNDARY-LAYER INTERACTION

Wakes interact with laminar boundary layers in many applications of engineering interest, for example on the leading edge of multi-component

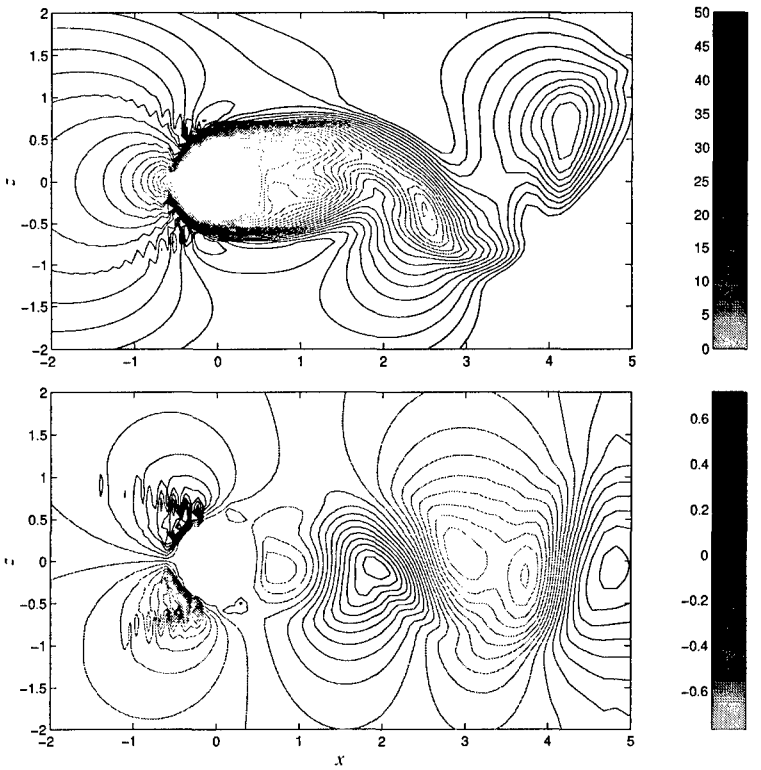

Figure 5. Flow over a circular cylinder, $Re_D = 300$. Coarse (200×100) 2D calculation. (a) Contours of the cell Reynolds number; (b) contours of w.

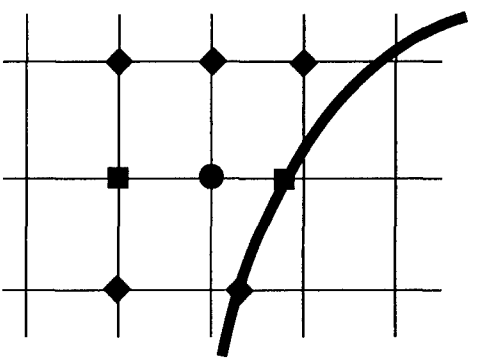

Figure 6. One-dimensional *vs.* two-dimensional interpolation stencils.

airfoils, or inside turbo-machinery. The interaction of the turbulent eddies present in the wake with the boundary layer itself then becomes a primary driver of the transition process in the boundary layer itself, and may lead

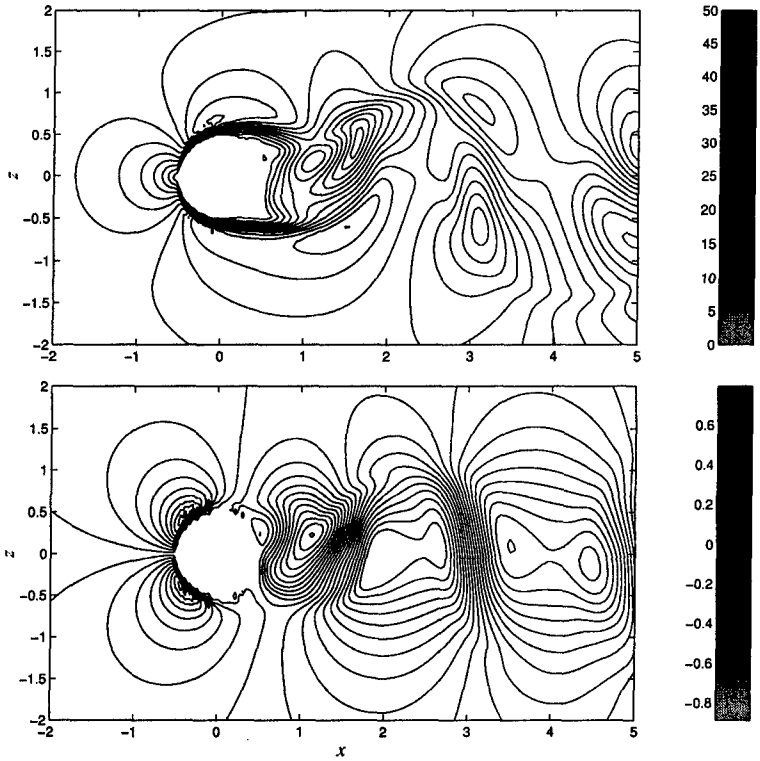

Figure 7. Flow over a circular cylinder, $Re_D = 300$. Fine (400 × 200) 2D calculation. (a) Contours of the cell Reynolds number; (b) contours of w.

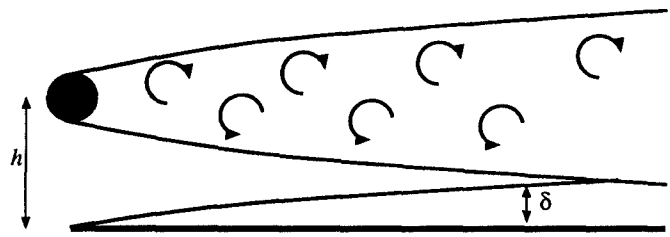

Figure 8. Sketch of the wake/boundary-layer configuration.

to transition to turbulence at fairly low Reynolds numbers.

The configuration examined in the present study is sketched in Fig. 8. A circular cylinder, with its axis normal to the stream is placed above a flat plate. The cylinder center is at $x_c = 10$, $z_c = 3.2$, immediately above the leading-edge of the plate, which was also at $x_c = 10$. As in the previous case, distances are normalized by D, velocities by U_∞. The computational

domain was $60 \times 2\pi \times 20$. As for the cylinder calculation, the grid was stretched both in the $x-$ and $z-$directions and a sponge region was used. The Reynolds number based on cylinder diameter was 385. The configuration corresponds to Case 1 in the experimental paper by Kyriakides *et al.* [7], who observed significant velocity fluctuations in the boundary layer, starting from a point approximately six diameters downstream of the cylinder. These fluctuations are generated by the large-scale convective motion of the vortices, and do not die down after the wake has weakened, but develop into a turbulent boundary layer despite the fact that the Reynolds number is very low.

The distribution of the streamwise Reynolds stress, $\langle u'u' \rangle$, as a function of x is shown in Fig. 9. A sudden increase of $\langle u'u' \rangle$ can be observed to begin at $x = 8$, indicating the beginning of transition. This result is consistent with the observations of Kyriakides *et al.* [7], who defined the onset of transition as "the $x-$location where the velocity signal at the same height above the plate loses its sinusoidal character", and found that transition occurs at $x = 7.4$.

The velocity profiles, shown in Fig. 10a at several locations, initially resemble a Blasius profile merging into a wake near the cylinder. As the wake widens and interacts with the boundary layer, a logarithmic layer begins to establish itself, indicative of transition towards turbulent flow. This transitional behavior is also observed in the trace of the Reynolds stress tensor, q^2 (equal to twice the turbulent kinetic energy), which in the latter sections establishes a turbulent-like distribution, with a peak of magnitude $7 - 8\tau_w$ at $z^+ \simeq 10 - 12$. It should be noted that this quasi-turbulent state is achieved at very low Reynolds number: the boundary-layer thickness δ (defined as the distance above the plate at which the first maximum of the velocity profile occurs) is approximately 50-70 wall units.

A visualization of the flow is shown in Fig. 11. The structure of the

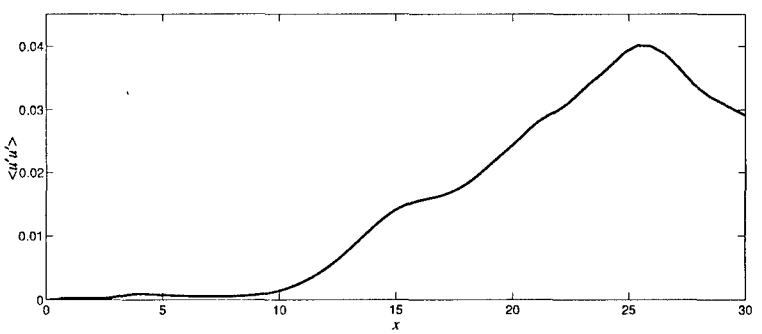

Figure 9. Wake/boundary-layer interaction. $\langle u'u' \rangle$ distribution at $z = 0.18$.

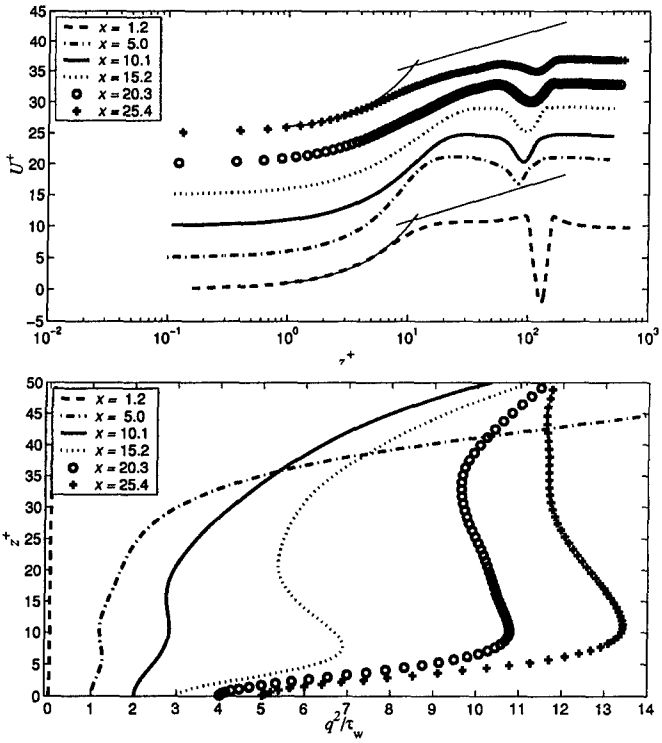

Figure 10. Wake/boundary-layer interaction. Turbulent statistics. Top: mean velocity profile; bottom: $q^2 = \langle u_i' u_i' \rangle$.

cylinder wake is similar to that highlighted in Fig. 4, with strong spanwise rollers that exhibit 3D instabilities and eventually break up, and smaller quasi-streamwise vortices in the braid region. The contours of streamwise velocity fluctuation u' on a plane parallel to the wall show significant levels of fluctuations, especially near kinks in the rollers belonging to the lower row. Quasi-streamwise streaks are formed around $x = 15$, whose spacing is approximately 100 wall units.

4. Conclusions

The immersed-boundary technique has been presented and discussed. Illustrative results from three simulations indicate the potential of this technique, which allows the calculation of flows around complex geometries without requiring a body-fitted grid.

If appropriate interpolation methods are used when the body does not coincide with a grid line, the method is second-order accurate. However, some care must be taken in the discretization of the flow field, especially in

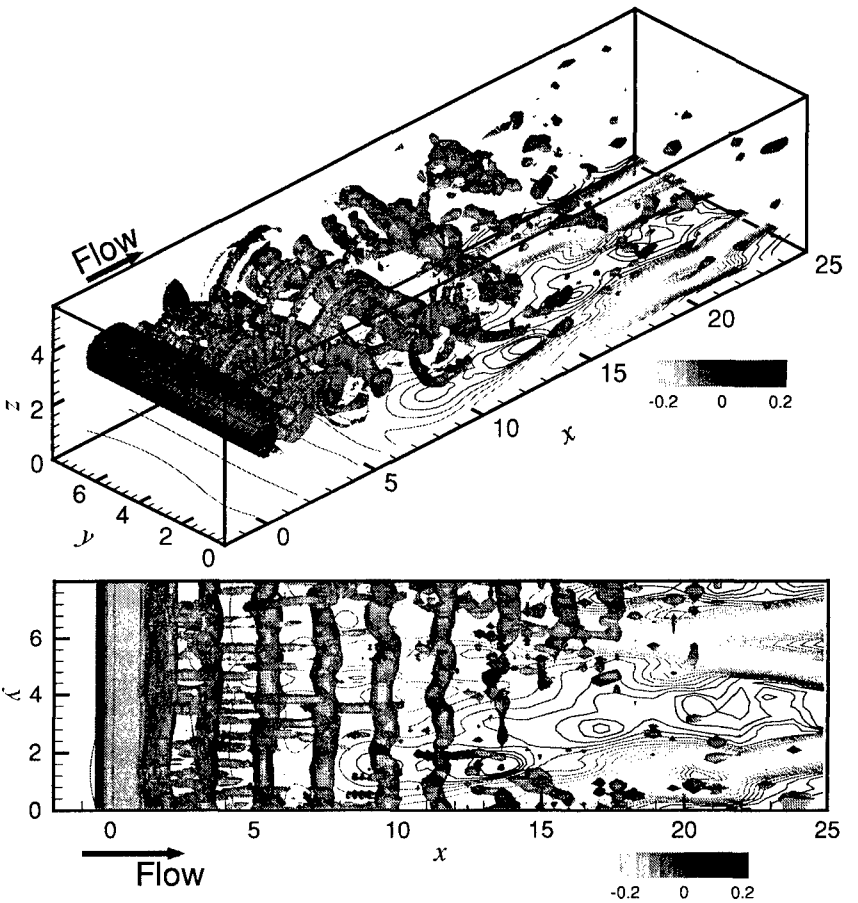

Figure 11. Wake/boundary-layer interaction. Isosurfaces of $Q = 0.4$ and contours of u' in the $z = 0.18$ plane. Top: perspective view; bottom: view from above.

the vicinity of the body. We have observed the development of numerical oscillations when the cell Reynolds-number exceeded values of approximately 30. These oscillations did not grow or change position in time, and their effect on the flow field downstream of the obstacle was limited in the cases studied. This was observed, for instance, in calculations of the flow around the cylinder at $Re_D = 3500$ were carried out in which the grid could not be sufficiently refined to satisfy the cell-Reynolds-number requirement. However, it is not known whether these oscillations might give rise to instabilities in other geometries, or at higher Reynolds numbers. The development of more accurate, multi-dimensional interpolation schemes might be beneficial in this respect. The use of multi-block methods, or embedded grids, could also alleviate this problem.

If these numerical schemes can be overcome, the immersed boundary

method appears to be a useful tool for the simulation of flows in complex geometries at moderate or high Reynolds numbers. This is confirmed by the increasing number of studies using this method that are appearing in the literature.

Acknowledgments

Research supported by the NASA Langley research Center under Grant NAG12285 monitored by Drs. Craig L. Streett and Meelan M. Choudhari.

References

1. Balaras, E. 1995 *Ph. D. Thesis*, EPFL (Federal Institute of Technology–Lausanne, Switzerland).
2. Chorin, A.J. 1968 *Math. Comput.* **22**, 745.
3. Fadlun, E.A., Verzicco, R., Orlandi, P., Mohd-Yusof, J. 2000 *J. Comput. Phys.* **161** 35.
4. Goldstein, D., Handler. R. Sirovich, L. 1993 *J. Comput. Phys.* **105**, 354–366.
5. Hunt, J.C.R., Wray, A.A. and Moin, P. 1988 In *Center for Turbulence Research, Proc. Summer Program 1988*, 193.
6. Kim, J. and Moin, P. 1985 *J. Comput. Phys.* **59** 308.
7. Kyriakides N.K., Kastrinakis, E.G., Nychas, S.G., Goulas, A. 1996 *Proc. Inst. Mech. Eng.* **210**, 167.
8. McQueen, D.M., Peskin, C.S. 1989 *J. Comput. Phys.* **82** 289.
9. McQueen D.M., Peskin, C.S. 1997 *J. Supercomput.* **11** 213.
10. Mittal, R. and Balachandar, S. 1995 *Phys. Fluids* **7**, 1841.
11. Mohd-Yusof, J. 1997 in *CTR Annu. Res. Briefs 1997*, NASA Ames/Stanford University, 317.
12. Orlanski, I. 1976 *J. Comput. Phys.* **21**, 251.
13. Peskin, C.S. 1972 *J. Comput. Phys.* **10** 252.
14. Peskin, C.S. 1977 *J. Comput. Phys.* **25** 220.
15. Verzicco, R., Mohd-Yusof, J., Orlandi, P., Haworth, D. 2000 *AIAA J.* **38** 427.
16. Wannier, G. H. 1950 *Quart. Applied Mathematics* **8** 1.